Bioinorganic Chemistry

DOI: 10.1002/anie.201208240

Nuclear Resonance Vibrational Spectroscopy and DFT study of Peroxo-Bridged Biferric Complexes: Structural Insight into Peroxo Intermediates of Binuclear Non-heme Iron Enzymes**

Kiyoung Park, Tomohiro Tsugawa, Hideki Furutachi, Yeonju Kwak, Lei V. Liu, Shaun D. Wong, Yoshitaka Yoda, Yasuhiro Kobayashi, Makina Saito, Masayuki Kurokuzu, Makoto Seto, Masatatsu Suzuki, and Edward I. Solomon**

Binuclear non-heme iron enzymes utilize O_2 to catalyze a variety of reactions, including hydrogen atom abstraction, desaturation, electrophilic aromatic substitution, and so on.[1] In most cases, their catalytic cycles begin with the reductive binding of O_2 by biferrous centers to form high-spin antiferromagnetically coupled (AFC) peroxo-bridged biferric intermediates.[2] These peroxo intermediates can either react with substrate or convert to more reactive high-valent species. Because of their transient nature, structural information must be deduced from spectroscopic data, which are rich for some peroxo intermediates, while for others too limited for geometric and electronic structural insight. The peroxo intermediate of W48F/D84E ribonucleotide reductase (RR), referred to as P, does exhibit distinct spectral features. These include electronic absorption (Abs) and resonance Raman (rR) spectra that are equivalent to those of cis μ-1,2 end-on peroxo-bridged Fe^{III}_2 model complexes, thus providing a basis for the computational model of P as a cis μ-1,2 peroxo-bridged Fe^{III}_2 species (with the $(Glu)_4(His)_2$ ligand set of this protein active site).[3] However, P is not reactive and must convert to a second-peroxo-level intermediate P′ that does not have Abs spectral features for rR-based structural elucidation.

For systems that do not have chromophores or are photoactive, nuclear resonance vibrational spectroscopy (NRVS) is an alternative to rR spectroscopy. NRVS is a synchrotron-based technique that probes vibrational side bands of ^{57}Fe nuclear transitions.[4–6] Its spectral intensity is determined by the amount of Fe displacement in each normal mode, thus allowing the specific investigation of the Fe active site with high sensitivity and without the limitation of the selection rules of rR spectroscopy. In this study, we establish the basis for the NRVS analysis of peroxo-bridged Fe^{III}_2 intermediates, based on structurally well-characterized synthetic model complexes. We have measured the NRVS spectra of $[Fe_2(\mu OH)(\mu O_2)(6Me_2\text{-}BPP)_2]^+$ (**1**) and $[Fe_2(\mu O)(\mu O_2)(6Me_2\text{-}BPP)_2]$ (**2**; Figure 1; $6Me_2$-BPP = *N*,*N*-bis(6-methyl-2-pyridylmethyl)-3-aminopropionate). These complexes are cis μ-1,2 peroxo-bridged species, the former with an additional hydroxo bridge and the latter with an oxo

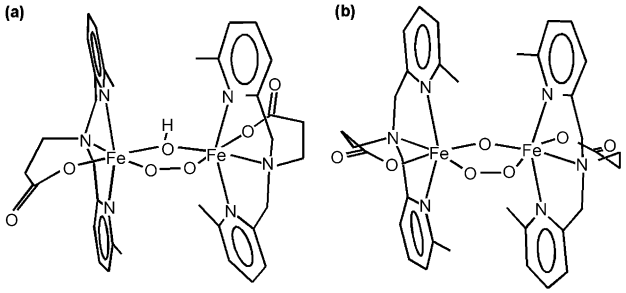

Figure 1. Schematic representations of a) **1** and b) **2**.

bridge.[7] We have assigned their NRVS spectral features, utilizing density functional theory (DFT) calculations in combination with normal coordinate analysis (NCA). Correlations between spectral and structural variations have been derived to elucidate spectral differences between **1** and prior data reported[8] and to establish a basis for structural elucidation of enzyme–peroxo intermediates.

The NRVS spectra of **1** and **2** (Figure 2a) are distinct from those of their starting materials, thus confirming homogeneity of the samples (Figure S1). The spectra display a major intense band that spans the region from 200 to 400 cm^{-1} (Figure 2a). This band is broader in **1** and down-shifted in energy from **1** (black) to **2** (gray), as their peaks are located at 221 and 202 cm^{-1}, respectively. In both spectra, the high-

[*] Dr. K. Park, Y. Kwak, L. V. Liu, Dr. S. D. Wong, Prof. Dr. E. I. Solomon
Department of Chemistry, Stanford University
Stanford, CA 94305-5080 (USA)
E-mail: edward.solomon@stanford.edu
T. Tsugawa, Prof. Dr. H. Furutachi, Prof. Dr. M. Suzuki
Department of Chemistry, Faculty of Science, Kanazawa University
Kakuma-machi, Kanazawa 920-1192 (Japan)
E-mail: suzuki@se.kanazawa-u.ac.jp
Dr. Y. Yoda
SPring-8/JASRI
1-1-1 Kouto, Sayo-cho, Sayo-gun, Hyogo 679-5198 (Japan)
Prof. Dr. Y. Kobayashi, Dr. M. Saito, M. Kurokuzu, Prof. Dr. M. Seto
Research Reactor Institute, Kyoto University
Kumatori-cho, Osaka 590-0494 (Japan)

[**] Use of the synchrotron radiation at the BL09XU of SPring-8 was approved by JASRI (proposal no. 2010B1569 and 2011A1326). Financial support for this research was provided by an NSF Biochemistry Program Grant (MCB-0919027 to E.I.S.), Grants-in-Aid for Scientific Research from the Ministry of Education, Culture, Sports, Science and Technology of Japan (22350027 to M. Suzuki and 23550071 to H.F.), and CREST, JST (to M. Seto).

Supporting information for this article is available on the WWW under http://dx.doi.org/10.1002/anie.201208240.

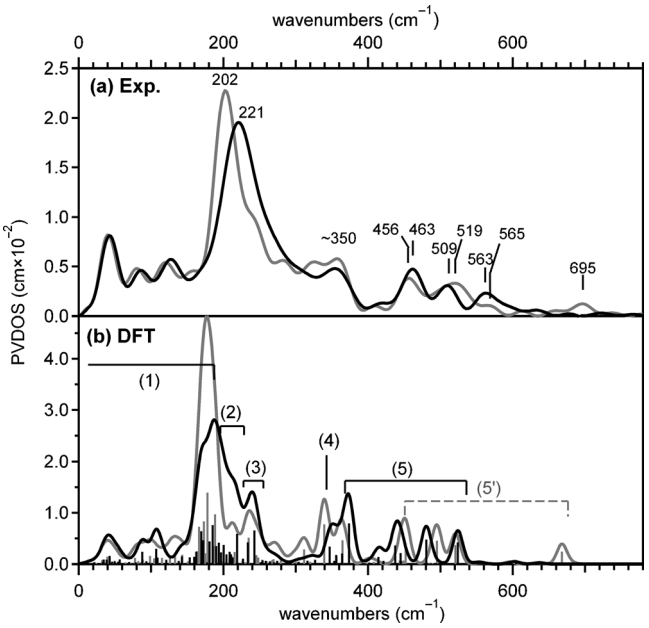

Figure 2. a) Experimental and b) DFT-calculated NRVS spectra of **1** (black) and **2** (gray). Bars are the mode factors of normal modes. PVDOS = partial vibrational density-of-states.

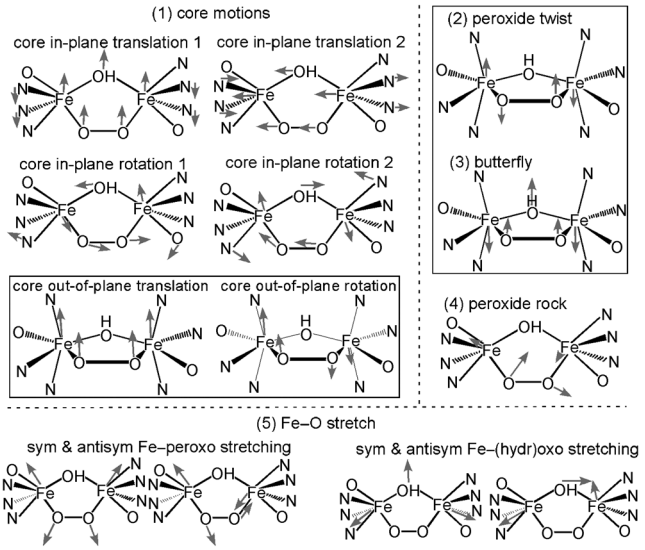

Figure 3. DFT-calculated vibrational modes of **1** and **2**. For clarity, only first-coordination-sphere motions are presented. Modes in frames are from the side view, while others are from the top view.

energy side of the band shows an additional weaker feature at around 350 cm^{-1}. At more than 400 cm^{-1}, three prominent peaks are observed at 463, 509, and 563 cm^{-1} in the spectrum of **1**, while **2** exhibits four peaks at 456, 519, 565, and 695 cm^{-1}. Considering the resolution of NRVS spectroscopy ($\approx$8 cm^{-1}) and $^{56/57}$Fe isotope shifts, the three peaks of **1** match with prior rR data (a Fermi doublet at 456 and 473 cm^{-1}, and two additional peaks at 498 and 548 cm^{-1}), and the NRVS peaks at 456 and 695 cm^{-1} of **2** were also observed in its rR spectrum.[7] Based on the rR enhancement by the μO_2-to-Fe charge-transfer band, the peak at around 460 cm^{-1} in both species has been assigned to the symmetric Fe–peroxide stretch, ν_s(Fe-μO_2).

To interpret these NRVS spectral features, the initial geometries of **1** and **2** obtained from crystal structures[7] were optimized using a spin-unrestricted DFT formalism with the 6-31G* basis set and the BP86 functional combined with 10% Hartree–Fock exchange (Figure 1). High-spin ferromagnetically coupled (FC) structures were obtained first and further optimized to get AFC structures. Both FC and AFC structures of **1** and **2** agree with their X-ray structures, although the {Fe_2O_2} core is slightly more expanded in the FC than in the AFC structure (see Table S1 and Figure S2 in the Supporting Information).

NRVS spectra predicted by DFT frequency calculations on the AFC structures successfully reproduce the experimental data, including the spectral differences between **1** and **2** (Figure 2b). Normal modes that contribute significantly to the NRVS spectra with high Fe displacements can be divided into five energy regions. First, the lower-energy side and the peak of the major band envelope at less than 190 cm^{-1} in the DFT-predicted spectra (Figure 2b, (1)) correlate with that at less than 220 cm^{-1} in the experimental spectra (Figure 2a). Region (1) contains the most intense features, involving a group of modes in which the {$Fe_2(\mu O_2)$} core translates or rotates without significant distortion (Figure 3(1), core motions). Region (2) at 200–220 cm^{-1} in the DFT-predicted spectra is associated with normal modes that contain out-of-plane peroxide bends, in which the two Fe atoms move in opposite directions (Figure 3(2), peroxide twist). On the higher energy side of the peroxide twist at 225–250 cm^{-1} (Figure 2b, (3)), there are modes involving out-of-plane peroxo bends, in which the two Fe atoms move in the same direction (Figure 3(3), butterfly). Regions (2) and (3) contribute to the band envelope between 220 and 325 cm^{-1} in Figure 2a. Region (4) is associated with a normal mode involving in-plane peroxide bends (Figure 3(4), peroxide rock), and contributes to the experimentally observed band at around 350 cm^{-1}. Region (5) consists of four Fe–O stretches, including symmetric and antisymmetric Fe–μO_2 and Fe–μO(H) stretches (Figure 3(5), Fe–O stretch). DFT calculations predict similar ν_s(Fe–μO_2) and ν_{as}(Fe–μO_2) for **1** and **2** (440 and 524 cm^{-1} for **1**; 451 and 521 cm^{-1} for **2**). Alternatively, ν_s(Fe–μO) and ν_{as}(Fe–μO) of **2** are predicted at 495 and 668 cm^{-1}, while those of **1** are down-shifted to 372 and 480 cm^{-1} as a result of the protonation of the oxo bridge. DFT calculations underestimated $\nu_{s/as}$(Fe–μO_2) and $\nu_{s/as}$(Fe–μO) compared to the rR and NRVS data, but qualitatively reproduce the experimental NRVS features at more than 400 cm^{-1} (i.e., three bands at 463, 509, and 563 cm^{-1} in the NRVS spectrum of **1** and four bands at 456, 519, 565, and 695 cm^{-1} in that of **2**).

Based on these DFT-assisted spectral assignments, the decrease in energy and narrowing of the major band at around 220 cm^{-1} from **1** to **2** (Figure 2a) reflects a decrease in energy of the core motions (region (1)) and decrease in intensity of the peroxo twist (region (2)). The DFT-optimized

structures of **1** and **2** show that the deprotonation of the hydroxo bridge results in strengthening of the resultant Fe–μO bonds and thus weakening of the bonds between Fe and the non-core terminal ligands (Figure S3). The stronger Fe–μO bonds restrain the Fe displacements of the peroxide twist, decreasing its NRVS intensity, while the weaker Fe–terminal ligand bonds decrease the frequencies of core motions that involve these stretch motions (Figure S4).

It should be noted that the previously reported NRVS spectrum of $[Fe_2(\mu O_2)(N\text{-EtHPTB})(PhCO_2)]^{2+}$ (**3**), which has a μ-1,2 end-on peroxide, a μ-alkoxide, and a carboxylate bridging two AFC ferric ions (Figure S5),[8] displays three major bands at 190, 275, and 330 cm^{-1}, rather than the one broad feature at less than 400 cm^{-1} observed for **1** and **2**. Consistently, the DFT-predicted NRVS spectrum of **3**, obtained using the same computational method as for **1** and **2**, also displays three features at 170, 220, and 280 cm^{-1} associated with regions (1), (2), and (3) of **1** (Figure 4a). One of the major differences between the DFT-optimized structure of **3** and that of **1** (and **2**) is that in **3**, the μO bridge is no longer in the $\{Fe_2(\mu O_2)\}$ plane (the angle between the $\{Fe_2\mu O\}$ plane and the $\{Fe_2(\mu O_2)\}$ plane $\theta = 155°$). Alternatively, if **3** is optimized as an FC rather than an AFC structure, it has a planar $\{Fe_2(\mu O)(\mu O_2)\}$ core as in **1** (Table S2) and its computed NRVS spectrum displays one broad band at less than 300 cm^{-1} (Figure 4b), similar to that of **1** (Figure 4c). Thus, the split three-peak pattern in the NRVS spectrum of **3** relative to **1** (and **2**) is associated with the decrease in planarity of the peroxo/hydroxo-bridged structure.

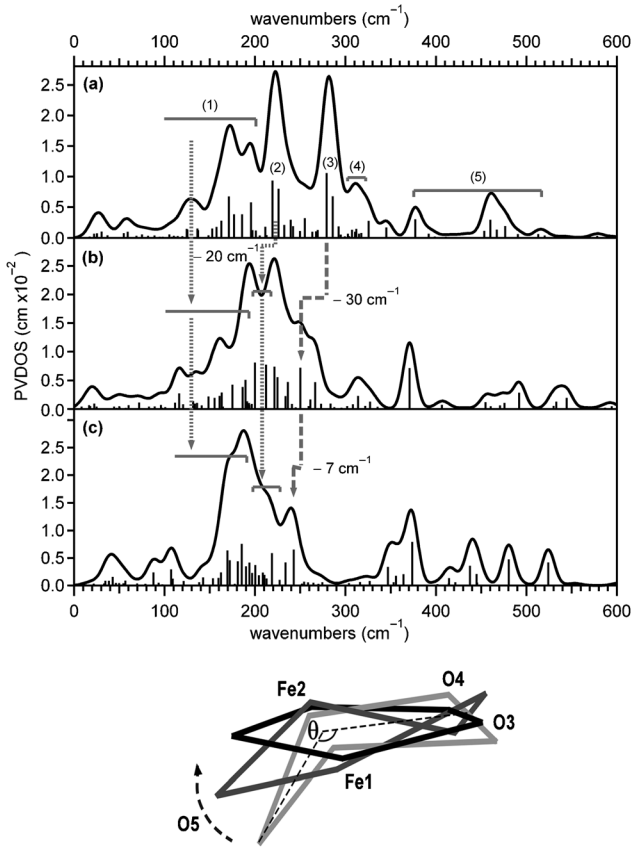

Figure 4. DFT-predicted NRVS spectra of a) **3**, b) FC **3**, and c) **1**. Inset shows variation in the planarity θ from **3** (gray, 126°) to FC **3** (dark gray, 155°) to **1** (black, 179°). From (a) to (c), regions (2) and (3) shift down in energy by around 20 and 30 cm^{-1}, respectively, with a decrease in intensity by approximately 60% of region (3).

This result indicates that the NRVS spectra of peroxo-bridged Fe^{III}_2 species are sensitive to the bridged core structure. We used a NCA approach to systematically evaluate the origin of this structural dependence of the NRVS data (Figure 5). Starting with the first-shell atoms of DFT-optimized **1**, the internal force constants were initially guessed from the DFT frequency calculation and then refined to fit the DFT-predicted NRVS spectrum (Figure 5a and Table S3). Three geometric perturbations were tested. First, a carboxylate bridge was added to the planar $\{Fe_2(\mu O)(\mu O_2)\}$ core. This perturbation significantly increases the intensity of the butterfly mode (by 80%, (3) in Figure 5b) but with a minor increase in energy (by 3.5 cm^{-1}), as the now present Fe–carboxylate bends contribute to the butterfly mode. Second, with the carboxylate bridge present, the planarity of the $\{Fe_2(\mu O)(\mu O_2)\}$ core, θ, was decreased from 179° to 111° (Figure 5c). This increases the frequency and intensity of the butterfly mode (by 12 cm^{-1} and 92%, (3) in Figure 5c). In the less-planar core, the butterfly mode involves increased contributions from Fe–equatorial ligand stretches and decreased contributions from μO-Fe-O_{axial}(N_{axial}) bends that have lower force constants (Table S4). Because of this increased stretch component in the less-planar core, the butterfly mode (3) exhibits increased amplitude of Fe motions as these bisect bonds (Figure S7). Additionally, the ν_s(Fe–μO) mode of the less-planar core involves out-of-plane Fe motion and thus Fe–μO_2 stretches, resulting in its increased frequency relative to that of the planar core (by 24 cm^{-1}). Finally, the increase of the Fe-O-O-Fe dihedral angle (ϕ) from 4° to 68° increases the energy of the peroxide twist (by 15 cm^{-1}; (2) in Figure 5d) and decreases that of the peroxide rock (by 37 cm^{-1}; (4) in Figure 5d). When the peroxide is distorted out of the $\{Fe_2(\mu O_2)\}$ plane, the peroxide twist gains more Fe–equatorial ligand stretch, and loses a contribution from μO_2-Fe-O_{axial}(N_{axial}) bend, resulting in its increased frequency. For the peroxide rock (4), an increase of ϕ shifts its composition from the higher-frequency Fe–μO_2 stretch to the lower-frequency Fe–axial ligand stretch, and thus reduces its frequency. Moreover, an up-shift of ν_s(Fe–μO_2) (by 38 cm^{-1}; Figure 5d) upon increase in ϕ was also seen in the rR study of $[Fe_2(\mu O_2)(OBz)_2\{HB(pz')_3\}_2]$.[9]

To summarize, the NRVS spectra of **1** and **2** can be divided into five regions. In order of increasing energy, the regions correspond to: (1) core motions (< 220 cm^{-1}), (2) peroxide twist (220–265 cm^{-1}), (3) butterfly (265–320 cm^{-1}), (4) peroxide rock (320–350 cm^{-1}), and (5) Fe–O stretches (> 350 cm^{-1}; Figure 2 and 3). The DFT and NCA calculations show that these five NRVS spectral features are sensitive to specific variations in the first-coordination-sphere structure. Region (1) shifts down in energy when the Fe–terminal ligand bonds are weakened. Region (2) shifts up in energy when the Fe-O-O-Fe dihedral angle (ϕ) increases, while region (4) shifts down for the same structural variation. For region (3), the frequency and NRVS intensity increase upon

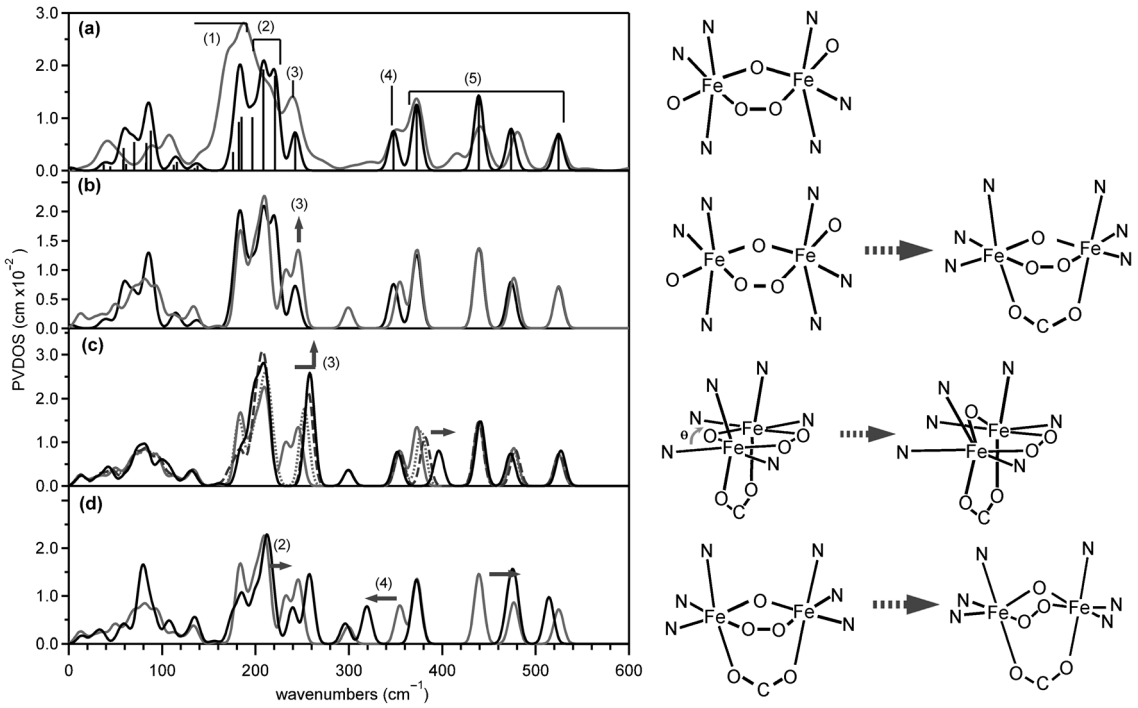

Figure 5. a) DFT-predicted NRVS spectrum of **1** (gray) and its NCA fit (black), b) NCA-predicted NRVS spectral changes upon addition of a carboxylate bridge (from black to gray), c) NCA-predicted NRVS spectral changes upon variation of θ from 179° (solid gray) to 164° (dotted gray) to 146°(dashed gray) and to 111° (black), and d) NCA-predicted NRVS spectral changes upon variation of ϕ from 4° (black) to 68° (gray).

the addition of a carboxylate bridge or with a decrease in the planarity of the core (θ). Finally, for region (5), ν_s(Fe–μO) increases with a decrease in θ, while ν_s(Fe–μO_2) increases as ϕ increases.

These results can now be extended to predict the NRVS spectrum of P based on its structure suggested by the prior Abs/rR study.[3] Its DFT-optimized structure was obtained by adding O_2 in a μ-1,2 end-on fashion to the biferrous structure that had been DFT-optimized from the crystal structure of *E. coli* biferrous RR[10] with α-carbon constraints, second-sphere residues, and one five-coordinate Fe, as calibrated by magnetic circular dichroism spectroscopy.[11] This P structure has two carboxylates bridging two high-spin AFC Fe^{III} atoms with θs of 111° and 109° relative to the {Fe_2(μO_2)} plane, which has a ϕ of 44° (Figure 6, inset). Its DFT-predicted NRVS spectrum displays three prominent features that are well-separated in energy ($\approx$170, $\approx$260, and $\approx$340 cm^{-1}). These features predicted for P correspond to regions (1)–(3) in **1**, but are at higher energy. Region (4) of P is predicted to be lower in energy than that of **1**, while the ν_s(Fe–μO_2) of P is at a similar energy to that of **1**, as observed in the rR studies.[3] These spectral perturbations for P relative to **1** reflect the above spectral/structural correlations. The higher energy of region (1) calculated for P relative to **1** can be attributed to its shorter and thus stronger Fe–carboxylate terminal bonds. The higher energy of region (2) combined with the down-shift in energy of region (4) calculated for P are consistent with the increase of ϕ from 3.5° (**1**) to 44° (P). Finally, the up-shift in energy of region (3) calculated for P relative to **1** reflects the replacement of the μOH bridge of **1** by a carboxylate bridge in P, which decreases the planarity θ from 179° (**1**) to 111° (P).

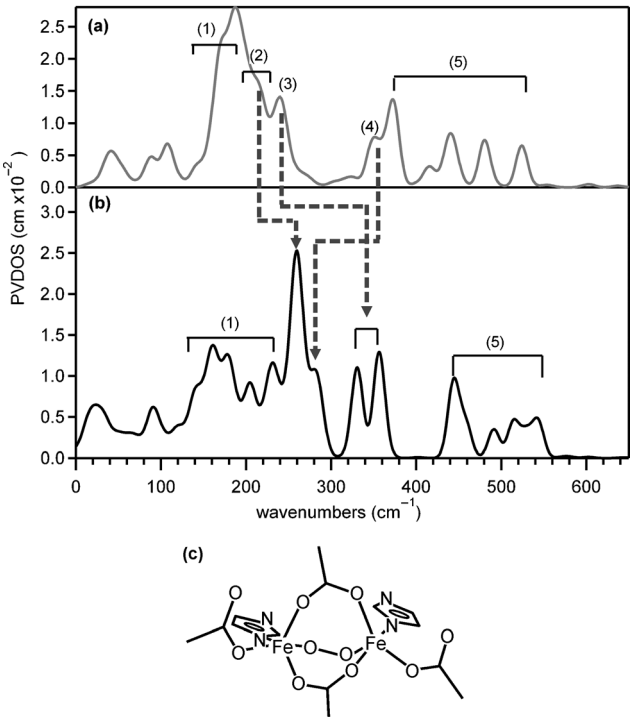

Figure 6. DFT-predicted NRVS spectra of a) **1** and b) P. c) DFT-optimized, first-sphere structure of P.

These correlations between NRVS spectral and geometric structural variations found in this study of high-spin peroxo–Fe^{III}_2 complexes can now be used as a basis for extracting structural information on peroxo intermediates in enzymes.

In particular, it will be important to evaluate the accuracy of the rR-predicted structure of P in W48F/D84E RR and to extend this correlation to other peroxo intermediates, including W48A/Y122F RR, which is the intermediate P′ activated for reduction to form X and for which rR has proved to be impossible.[12]

Experimental Section

Samples were prepared as previously described.[7] NRVS spectra were collected at BL09XU, SPring-8, and processed using the PHOENIX program.[13] DFT and NCA calculations were performed using the Gaussian '09 package and the Vibratz 2.3 package, respectively (see the Supporting Information).

Received: October 12, 2012
Published online: December 6, 2012

Keywords: binuclear complexes · bioinorganic chemistry · iron · peroxo intermediate · structure elucidation

[1] B. J. Wallar, J. D. Lipscomb, *Chem. Rev.* **1996**, *96*, 2625 – 2657.
[2] E. I. Solomon, T. C. Brunold, M. I. Davis, J. N. Kemsley, S. K. Lee, N. Lehnert, F. Neese, A. J. Skulan, Y. S. Yang, J. Zhou, *Chem. Rev.* **2000**, *100*, 235 – 349.
[3] A. J. Skulan, T. C. Brunold, J. Baldwin, L. Saleh, J. M. Bollinger, Jr., E. I. Solomon, *J. Am. Chem. Soc.* **2004**, *126*, 8842 – 8855.
[4] M. Seto, Y. Yoda, S. Kikuta, X. W. Zhang, M. Ando, *Phys. Rev. Lett.* **1995**, *74*, 3828 – 3831.
[5] W. Sturhahn, T. S. Toellner, E. E. Alp, X. W. Zhang, M. Ando, Y. Yoda, S. Kikuta, M. Seto, C. W. Kimball, B. Dabrowski, *Phys. Rev. Lett.* **1995**, *74*, 3832 – 3835.
[6] W. Sturhahn, *J. Phys. Condens. Matter* **2004**, *16*, S497 – S530.
[7] X. Zhang, H. Furutachi, F. Shuhei, N. Shigenori, Y. Maeda, Y. Watanabe, T. Kitagawa, M. Suzuki, *J. Am. Chem. Soc.* **2005**, *127*, 826 – 827.
[8] L. H. Do, H. Wang, C. E. Tinberg, E. Dowty, Y. Yoda, S. P. Cramer, S. J. Lippard, *Chem. Commun.* **2011**, *47*, 10945 – 10947.
[9] T. C. Brunold, N. Tamura, N. Kitajima, Y. Moro-oka, E. I. Solomon, *J. Am. Chem. Soc.* **1998**, *120*, 5674 – 5690.
[10] W. C. Voegtli, M. Sommerhalter, L. Saleh, J. Baldwin, J. M. Bollinger, Jr., A. C. Rosenzweig, *J. Am. Chem. Soc.* **2003**, *125*, 15822 – 15830.
[11] Y. S. Yang, J. Baldwin, B. A. Ley, J. M. Bollinger, Jr., E. I. Solomon, *J. Am. Chem. Soc.* **2000**, *122*, 8495 – 8510.
[12] L. Saleh, C. Krebs, B. A. Ley, S. Naik, B. H. Huynh, J. M. Bollinger, Jr., *Biochemistry* **2004**, *43*, 5953 – 5964.
[13] W. Sturhahn, *Hyperfine Interact.* **2000**, *125*, 149 – 172.

